

Non-Clifford diagonalization for measurement shot reduction in quantum expectation value estimation

Nicolas PD Sawaya,^{1,*} Daan Camps,² Ben DalFavero,³ Norm M Tubman,⁴ Grant M Rotskoff,⁵ and Ryan LaRose^{3,†}

¹*Azulene Labs, San Francisco, CA 94115*

²*National Energy Research Scientific Computing Center, Lawrence Berkeley National Laboratory, Berkeley, California, USA*

³*Center for Quantum Computing, Science, and Engineering, Michigan State University, East Lansing, MI 48823, USA*

⁴*NASA Ames Research Center, Moffett Field, CA, 94035, USA*

⁵*Department of Chemistry, Stanford University, Stanford, California 94305, USA*

(Dated: July 2, 2025)

Estimating expectation values on near-term quantum computers often requires a prohibitively large number of measurements. One widely-used strategy to mitigate this problem has been to partition an operator’s Pauli terms into sets of mutually commuting operators. Here, we introduce a method that relaxes this constraint of commutativity, instead allowing for entirely arbitrary terms to be grouped together, save a locality constraint. The key idea is that we decompose the operator into arbitrary tensor products with bounded tensor size, ignoring Pauli commuting relations. This method — named k -NoCliD (k -local non-Clifford diagonalization) — allows one to measure in far fewer bases in most cases, often (though not always) at the cost of increasing the circuit depth. We introduce several partitioning algorithms tailored to different Hamiltonian classes. For electronic structure, we numerically demonstrate the existence of threshold values of k for which k -NoCliD leads to the lowest shot counts, though we leave improved partitioning algorithms to future work. We focus primarily on three Hamiltonian classes—molecular vibrational structure, Fermi-Hubbard, and Bose-Hubbard—and show that k -NoCliD reduces the number of circuit shots, often by a very large margin, and often even for k as small as 2.

CONTENTS

I. INTRODUCTION

I. Introduction	1
II. Theory	2
A. k -local non-Clifford diagonalization	2
B. Illustrative example	3
C. Hamiltonian classes	4
D. Partitioning via greedy algorithm	5
E. Blocking with residuals	5
F. Index reordering	5
G. Partitioning via pre-encoded operators	6
H. Lattice edge coloring	6
I. Products of one-body Hermitians	6
J. Sub-operators	7
III. Numerical results	7
IV. Conclusions	8
Acknowledgements	9
A. Valid and invalid tensor products for k -NoCliD	9
B. Proof of 1-qubit basis change result	10
References	11

Calculating expectation values of observables is a ubiquitous subroutine in quantum computing [1–3]. Importantly, for some application areas like chemistry and materials science [4–6], an enormous number of measurements (i.e. circuit repetitions or circuit “shots”) are required to estimate expectation values to reasonable accuracy [7–10].

In qubit space, the Hamiltonian of interest can be represented as a linear combination of Pauli terms,

$$H = \sum_i c_i P_i, \quad (1)$$

where $P_i \in \{I, X, Y, Z\}^{\otimes n}$, n is the number of qubits, $\{I, X, Y, Z\}$ are the Pauli matrices, and c_i are real coefficients.

Several algorithms have been developed for reducing the number of circuit shots required [7, 9, 11–22]. Perhaps the most widely used class of algorithms for shot reduction is based on partitioning H into sets of commuting Pauli terms [7, 9, 13, 23, 24]. Both the commutation locality (qubit-wise commuting [12], k -qubitwise [22], or fully commuting [13]) and the partition algorithm (e.g. SortedInsertion [7] or graph-based methods [12]) have been studied. Such partitioning strategies have been shown to reduce the shot counts by orders of magnitude, though even after this reduction the required shots may be prohibitive [8].

Here we introduce a novel partition-and-diagonalize strategy that does *not* require the Pauli terms in each partition to commute. We introduce the k -NoCliD (k -local non-Clifford diagonalization) algorithm. The basic

* nicolas@azulene.com

† rmlarose@msu.edu

idea is to transform equation (1) into a partition of product states of arbitrarily sized tensors, and measure in the basis of each individual tensor product. This allows one to measure in far fewer bases and leads to far fewer circuit shots in many cases, as we numerically demonstrate for a broad set of Hamiltonians.

II. THEORY

A quantum operator may be expressed as

$$H = \sum_{q=1}^K h_q, \quad (2)$$

such that each operator h_q may be measured in a single basis, with many circuit shots yielding an estimate for $\langle h_q \rangle$. At this point, equation (2) makes no assumptions whatsoever about the form of h_q . (If the Hamiltonian is expressed as a weighted Pauli string as in equation (1), a commonly used strategy is to group Pauli strings P_i that satisfy some mutual commutativity relation into the same operator h_q , as discussed below.) The general expression for total measurements N_{tot} required for error ε on $\langle H \rangle$ is [7]

$$\varepsilon^2 N_{tot} = \left(\sum_{q=1}^K \sqrt{\text{Var}[h_q]} \right)^2. \quad (3)$$

In this work we focus on expectation value methods where shot counts scale as $O(1/\varepsilon^2)$, which are appropriate for nearer-term NISQ algorithms. We do not consider $O(1/\varepsilon)$ -scaling methods [25–27], which are appropriate for long-term error-corrected quantum computers as they require much longer circuit depths.

The most widely-used methods [7, 9, 13] for estimating $\langle H \rangle$ have required that each h_q be a superposition of Pauli strings P_i that mutually commute. In this work we remove this constraint, allowing for measurement in an arbitrary “non-Pauli” basis. One consequence is that the basis-change circuits are no longer Clifford circuits [7]; hence we call the method k -NoCliD, for k -local non-Clifford diagonalization.

To begin justifying this approach of measuring in a non-Pauli basis, it is instructive to consider a one-qubit example. We consider a real Hamiltonian and real state, *i.e.* we constrain ourselves to the XZ plane. Consider the Hamiltonian

$$H_\eta = \eta X + \sqrt{1 - \eta^2} Z, \quad (4)$$

a unit-norm one-qubit operator for which the eigenvectors lie along an angle $\arccos \eta$ relative to the Z axis. Then, we compare the traditional approach of measuring in two bases (X and Z bases) before reconstructing $\langle H_\eta \rangle = \eta \langle X \rangle + \sqrt{1 - \eta^2} \langle Z \rangle$, versus measuring “directly” in just one non-Pauli bases or “rotated basis” $P_{H_\eta} = H_\eta$ (note that P_{H_η} has unit norm, $P_{H_\eta} = I$). The latter is

done by performing a rotation around the Y axis by an angle $\arccos \eta$ before measurement.

Appendix B provides additional pedagogical discussion, where we also prove the following result. For a given error, N_{tot}^{GPB} is the number of shots required when using the global Pauli basis, *i.e.* reconstructing $\langle H \rangle$ from $\langle X \rangle$ and $\langle Z \rangle$. N_{tot}^{RB} is the number of shots when measuring in the single rotated basis $\langle H_\eta \rangle$.

Result 1. *Consider evaluating $\langle \psi | H | \psi \rangle$ for a Hamiltonian $H_\eta = \eta X + \sqrt{1 - \eta^2} Z$ with $\eta \in [0, 1]$ and any real state $|\psi\rangle = \alpha |0\rangle + \sqrt{1 - \alpha^2} |1\rangle$, where the rotated basis is $P_{H_\eta} = H_\eta$. For all η and α , $N_{tot}^{RB} \leq N_{tot}^{GPB}$. Hence, in terms of shot counts, it is always optimal to measure in this rotated non-Pauli basis.*

This finding for the simple one-qubit case motivates this work, where we explore whether using arbitrary non-Pauli bases is beneficial in larger problems.

A. k -local non-Clifford diagonalization

The procedure of k -NoCliD begins with refactoring the Hamiltonian into L operators as

$$H = \sum_{q=1}^L M_q, \quad (5)$$

where the key point is that each M_q may be measured in a single basis and one would usually like to have $L \ll K$. The structure of each M_q is discussed below. Thus one measures in L bases in order to reproduce $\langle H \rangle = \sum_q \langle M_q \rangle$. To evaluate each $\langle M_q \rangle$ on a quantum computer, it is necessary to diagonalize each M_q operator as

$$M_q = U_q D_q U_q^\dagger. \quad (6)$$

Given many copies of the state of interest $|\psi\rangle$ — prepared for example by variational quantum eigensolver (VQE) [28] and sometimes denoted $|\psi\rangle = U_{VQE} |0\rangle$ — to calculate $\langle M_q \rangle$ one must execute a quantum circuit for U_q^\dagger . This procedure leads to

$$\begin{aligned} \langle M_q \rangle &= \langle \psi | U_q U_q^\dagger M_q U_q U_q^\dagger | \psi \rangle \\ &= \langle \psi | U_q D_q U_q^\dagger | \psi \rangle. \end{aligned} \quad (7)$$

Hence after implementing the change-of-basis circuit U_q^\dagger , the calculation of $\langle M_q \rangle$ has been transformed to a calculation of $\langle D_q \rangle$, which can now be performed in the computational Z basis because D_q is diagonal. Note that in a full implementation one must consider the cost to compile the circuit unitary U_q on a classical computer. The estimator for the Hamiltonian is then

$$\langle H \rangle = \sum_q \langle M_q \rangle = \sum_q \langle \psi | U_q D_q U_q^\dagger | \psi \rangle. \quad (8)$$

Previously proposed shot reduction methods [7, 9, 13] may be expressed as equation (5) (though they are not always expressed as such). For example, in fully commuting (FC) partitioning, $M_q = \sum_{P_j \in \mathcal{R}_q} c_j P_j$, where all P_j in the set \mathcal{R}_q mutually commute [9, 13]. In FC, the diagonalization circuit U_q^\dagger is always a Clifford circuit requiring at most depth $O(n^2/\log n)$ gates [29]. By contrast, in k -NoCliD, U_q^\dagger is *not* constrained to be a Clifford circuit, which can lead to large reductions in shot counts, as demonstrated in our numerical section. Because we lose the guarantee that the depth scales quadratically, shot count reduction often comes with an increase in circuit depth. Generally, we write the circuit depth is $O(f(k))$ for some function $f(k)$. While compiling arbitrary unitaries results in $f(k) \sim 2^k$ [30, 31], this may often be an overly pessimistic estimate because the operators to diagonalize in problems of interest are often highly structured (for example strings of bosonic position operators $q_i \otimes q_j \otimes \dots$). Furthermore, often the circuit depth will not increase (or the increase will be manageable) because k -NoCliD is intended to be implemented with $k \ll n$. This will often lead to $O(f(k))$ being less than $O(n^2/\log(n))$. Further, while n increases with system size by definition, k -NoCliD will often lead to k being naturally bounded by a constant, especially for bosonic and phononic Hamiltonians, but also for the greedy and blocking algorithms introduced below.

We now discuss the specific structure of M_q that is used in k -NoCliD. The M_q are chosen such that they can be factorized as

$$M_q = \sum_{r=1}^{l_q} W_{qr} \quad (9)$$

where each W_{qr} is a tensor product

$$W_{qr} = A_{qr1}^{\mathcal{K}_{qr1}} \otimes A_{qr2}^{\mathcal{K}_{qr2}} \otimes A_{qr3}^{\mathcal{K}_{qr3}} \otimes \dots \quad (10)$$

such that \mathcal{K}_{qrs} is the set of number of qubits over which the local tensor acts, and we require the cardinality of each set to be $|\mathcal{K}_{qrs}| \equiv k_{qrs} \leq k$. The k_{qrs} may be unequal but they must all be at most k , and for any tensor product W_{qr} we have $\sum_s k_{qrs} = n$, the number of qubits. Note that equation (10) does not require qubits to be adjacent. All tensor products W_{qr} in the same partition q must commute with each other, $\forall(r, r') : [W_{qr}, W_{qr'}] = 0$; this constraint is what allows $\langle M_q \rangle$ to be measured in a single basis. Note that W_{qr} is not restricted to be a Pauli term, so this commutation constraint is not the same as the one used in traditional shot reduction [13]. For example, for 2-NoCliD, $W_{qr} = (X_1 X_2 + Y_1 + Z_1) \otimes (Y_3 Z_4)$ and $W_{qr'} = (X_1 X_2 + Y_1 + Z_1) \otimes (I_3 I_4)$ do obey this constraint, where subscripts denote qubit index.

The key benefit of the method is that one need measure in only L bases (one for each M_q), where L can be made to be much smaller than the number of partitions (*i.e.* fragments) required in traditional methods. This in turn can lead to large reductions in shot counts. Note

that a smaller number of fragments does not automatically guarantee lower shot counts [9]—numerical results, provided below, are required to confirm that any given partitioning indeed leads to lower shot counts.

Because for a given q all W_{qr} commute, they are simultaneously diagonalizable. This work’s numerical implementation will assume that *tensor-wise commutation* holds, such that in a tensor product each tensor can be diagonalized independently. (A counter-example would be $q_i q_j$ and $p_i p_j$ where q and p are respectively bosonic position and momentum operators—the terms commute but they require diagonalization across two tensors). This constraint makes the formalism easier but it is not required for k -NoCliD. Thus the diagonalization unitaries take the form

$$U_q = V_{q,1} \otimes V_{q,2} \otimes \dots \quad (11)$$

where all V are unitary and tensor sizes match those in equation (10). For a given M_q , one can then implement all V in parallel. Each V may be decomposed into a gate set via a variety of circuit compilation methods [30–32]. The choice of k is arbitrary; a larger k will usually lead to fewer circuit shots but more circuit depth.

Note that the k -NoCliD construction has one more “layer” of complexity than commonly used methods like QWC and full-commuting partitioning: we partition the Hamiltonian into distinct M_q operators, which are in turn partitioned into multiple W_{qr} , which in turn may be represented as sums of Pauli strings.

Formally stated, in k -NoCliD the optimal partitioning for a Hamiltonian H is

$$\begin{aligned} & \arg \min_{\{W_{qr}\}} \sum_{q=1}^L \sqrt{\text{Var}[M_q]} \\ & = \arg \min_{\{W_{qr}\}} \sum_{q=1}^L \sqrt{\text{Var}[\sum_r W_{qr}]} \end{aligned} \quad (12)$$

subject to the constraints

$$\begin{aligned} & \sum_q W_{qr} = H \\ & \forall k_{qri} : k_{qri} \leq k \\ & \forall(q, r, r') : [W_{qr}, W_{qr'}] = 0. \end{aligned} \quad (13)$$

This optimization is over a continuous space, since multiple W tensors may include some component of the same Pauli string P_i with arbitrary coefficient, and since a Pauli string not present in H may be included as long as they cancel out in the overall sum [18, 19]. Finding the optimal partitioning is a hard problem and we introduce heuristic methods to find a reasonable partitioning.

B. Illustrative example

Now that we have introduced the general method, let us now consider an example to illustrate the idea and

advantage of the approach. Consider the following (artificial) four-qubit Hamiltonian

$$H = I + \frac{1}{2}X_0X_1X_2 + X_0X_2 + \frac{1}{2}Y_0Y_1X_2 + X_1 + 2X_1X_2 + X_1X_2X_3 - X_1X_2Z_3 - X_1Z_2 - \frac{1}{2}X_1Z_2X_3 + \frac{1}{2}X_1Z_2Z_3 + \frac{1}{2}X_1X_3 - \frac{1}{2}X_1Z_3 + 4X_2 + X_2X_3 - X_2Z_3 - Z_2 - \frac{1}{2}Z_2X_3 + \frac{1}{2}Z_2Z_3 + \frac{1}{2}X_3 - \frac{1}{2}Z_3. \quad (14)$$

Implementing the SortedInsertion [7] algorithm with full commutation yields five sets of mutually commuting Pauli terms:

$$\begin{aligned} &\{X_2, X_1X_2, X_2X_3, X_1X_2X_3, X_1, X_0X_2, X_3, X_1X_3, \\ &\quad X_0X_1X_2\}; \{Z_2, X_1Z_2, Z_2X_3, X_1Z_2X_3\}; \\ &\quad \{Z_2Z_3, X_1Z_2Z_3\}; \quad (15) \\ &\{X_2Z_3, X_1X_2Z_3, Z_3, X_1Z_3\}; \\ &\quad \{Y_0Y_1X_2\}. \end{aligned}$$

Hence one can evaluate $\langle H \rangle$ using *five* measurement bases. Next we consider k -NoCliD. With 2-NoCliD, there exists the following decomposition into just *two* measurement bases $M_1 = W_{11} + W_{12}$ and $M_2 = W_{21}$, where

$$\begin{aligned} W_{11} &= \begin{pmatrix} 1 & 0 & 1 & 0 \\ 0 & 1 & 0 & 1 \\ 1 & 0 & 1 & 0 \\ 0 & 1 & 0 & 1 \end{pmatrix} \otimes \begin{pmatrix} 0 & 1 \\ 1 & 1 \end{pmatrix} \otimes \begin{pmatrix} 0 & 1 \\ 1 & 2 \end{pmatrix} \\ W_{12} &= \begin{pmatrix} 1 & 0 & 1 & 0 \\ 0 & 1 & 0 & 1 \\ 1 & 0 & 1 & 0 \\ 0 & 1 & 0 & 1 \end{pmatrix} \otimes \begin{pmatrix} 0 & 1 \\ 1 & 1 \end{pmatrix} \otimes \begin{pmatrix} 1 & 0 \\ 0 & 1 \end{pmatrix} \quad (16) \\ W_{21} &= \begin{pmatrix} 2 & 1 & 0 & 0 \\ 1 & 2 & 1 & 0 \\ 0 & 1 & 2 & 1 \\ 0 & 0 & 1 & 2 \end{pmatrix} \otimes \begin{pmatrix} 0 & 1 \\ 1 & 0 \end{pmatrix} \otimes \begin{pmatrix} 1 & 0 \\ 0 & 1 \end{pmatrix}. \end{aligned}$$

Although, as mentioned, the number of measurement bases does not always correlate with the number of shots needed, this example illustrates how relaxing Clifford constraints in k -NoCliD yields fewer measurement bases, which could potentially decrease the number of shots. Indeed, in our numerical results below we directly study the effects of this new partitioning scheme on shot counts and show an advantage in k -NoCliD in several applications of interest.

C. Hamiltonian classes

Here we summarize the four Hamiltonian classes considered in this work. They include problems with either bosonic or fermionic commutation relations. Though the

methods we discuss here are general to any quantum operator, we introduce these Hamiltonian classes here because we discuss many of our methods explicitly in terms of these common Hamiltonians.

The spinless Fermi-Hubbard [33–35] lattice model is defined as

$$H = - \sum_{\langle i,j \rangle} t_{ij} (a_i^\dagger a_j + a_j^\dagger a_i) + \sum_{\langle i,j \rangle} \frac{U_{ij}}{2} a_i^\dagger a_i a_j^\dagger a_j \quad (17)$$

where i and j denote lattice sites, t_{ij} are hopping terms, and U_{ij} are repulsion terms. We consider only models with nearest-neighbor interactions.

The molecular electronic structure Hamiltonian is defined as

$$H = \sum_{pq} t_{pq} a_p^\dagger a_q + \frac{1}{2} \sum_{pqrs} t_{pqrs} a_p^\dagger a_q^\dagger a_r a_s. \quad (18)$$

where orbitals are labelled p, q, r, s . In this work, for both Fermi-Hubbard and electronic structure, we implement only the Jordan-Wigner transformation [36, 37].

The Bose-Hubbard model [38–40] describes bosonic particles on a lattice,

$$H_{BH} = - \sum_{\langle i,j \rangle} t_{ij} (b_i^\dagger b_j + h.c.) + \sum_i \frac{U_i}{2} n_i (n_i - 1) \quad (19)$$

where i and j denote lattice sites, t_{ij} are hopping terms, and U_i is the on-site interaction.

Many chemical processes and properties depend on the behavior of the nuclei, as described by a molecular vibrational Hamiltonian [41–44]. One uses standard bosonic operators to produce a Hamiltonian

$$\begin{aligned} H_v &= \frac{1}{2} \sum_i^M \omega_i (q_i^2 + p_i^2) \\ &\quad + \sum_{\{ijk\}} t_{ijk} q_i q_j q_k \\ &\quad + \sum_{\{ijkl\}} t_{ijkl} q_i q_j q_k q_l + \dots, \end{aligned} \quad (20)$$

where indices label the vibrational mode and the expansion is to arbitrarily high order. Though we use the harmonic basis, other bases may be used. While H_v is classically solvable for some molecules, in general the anharmonic coupling terms lead to this being a hard problem, as discussed elsewhere [45].

A notable property of bosonic and vibrational problems is their canonical bosonic commutation relations, because (unlike in the fermionic case) this leads to qubit-encoded Hamiltonians that have the same tensor-product structure as the bosonic Hamiltonian. As we discuss below, this allows one to use tensor products of $\{q_i\}$, $\{p_i\}$, and $\{n_i\}$ as the measurement basis for *any* bosonic or phononic problem instance. For encoding [42, 46–48] bosonic and phononic modes we used the Gray code [49, 50].

We note that expectation value estimation is a required subroutine for some near-term quantum algorithms for classical problems as well [51–58]. However, for this work we focus entirely on quantum problems.

D. Partitioning via greedy algorithm

Here we describe the first of our k -NoCliD partitioning methods, a simple greedy algorithm that operates on the encoded (qubit space) Hamiltonian. Pseudocode for the greedy algorithm is given here:

```

▷ FREEQUBITS() returns the number of mismatched
qubits, where the local Pauli is different on different
qubits.
▷ DISJOINT() returns true only if the inputs operate
on disjoint qubits.
for  $P_i$  in  $\{P_i \text{ ordered by } |c_i| \text{ descending}\}$  do
  for  $M_q$  in  $\{M_q\}$  do
    for  $W_{qr}$  in  $\{W_{qr}\}$  do
      if  $\text{FREEQUBITS}(W_{qr}, P_i) \leq k$  then
         $W_{qr} = W_{qr} + P_i$ 
        break 2 loops
      end if
      if  $P_i$  rejected from all  $W_{qr}$  then
        if  $\text{DISJOINT}(W_{qr}, P_i)$  for all  $W_{qr}$  then
          Initialize new  $W_{q,r+1} = P_i$ 
          break 2 loops
        end if
      end if
    end for
  end for
end for
if  $P_i$  rejected from all  $\{M_q\}$  then
  Initialize new  $M_{q+1}$ 
  Add  $W_{q+1,1} = P_i$  to  $M_{q+1}$ 
end if
end for

```

The basic idea is to loop through terms of the qubit-encoded operator, determining how many mismatched qubits are present in a given W_{qr} . These (at most k) “free qubits” are the ones across which a diagonalization unitary will be placed. If an attempt to place a term P_i into W_{qr} leads to more than k mismatched qubits, then the algorithm attempts to form a new $W_{q,r+1}$ in partition M_q . This attempt succeeds only if W_{qr} and P_i operate on disjoint qubits; otherwise, an attempt is made to place P_i into M_{q+1} . Only after placement attempts fail for all M_q is a new $M_{q'}$ created.

The P_i are looped through in descending order of importance, by magnitude of c_i , as in the SortedInsertion approach [7]. Note, requiring that W_{qr} and $W_{qr'}$ (with $r \neq r'$) operate on disjoint qubits is a significant restriction that was imposed only for ease of implementation; removing this restriction would lead to fewer partitions.

E. Blocking with residuals

Here we introduce a second partitioning method that also operates directly on the qubit-encoded Hamiltonian. The main idea is to partition the qubits into sets of size at most k , and then pack as many operators as possible into those qubit sets. After several iterations, the remaining unassigned terms (which we call the residual) in the qubit Hamiltonian, which will tend to be longer Pauli strings, are treated with a separate method.

For the blocking method we define an arbitrary number of bases M_q^B . These are constructed in ascending order (M_0^B before M_1^B , etc.). M_i is constructed by defining a disjoint collection of sets, where each set $\mathcal{K}_q^{(1)}, \mathcal{K}_q^{(2)}, \dots$ contains at most k qubit indices

$$M_q^B = C_q^{\mathcal{K}_q^{(1)}} \otimes C_q^{\mathcal{K}_q^{(2)}} \otimes C_q^{\mathcal{K}_q^{(3)}} \otimes \dots \quad (21)$$

such that any $C_q^{\mathcal{K}_q^{(s)}}$ contains all remaining terms that operate exclusively on qubits in $\mathcal{K}_q^{(s)}$ (“remaining” because some operators may have already been placed in a previous M_j with $j < q$).

Though the only constraint is that $|\mathcal{K}_i| < k$ for all i , for this work we use contiguous sets of qubits for this blocking algorithm (this is not the case for our greedy algorithm). For M_1^{SS} , we use $\mathcal{K}_1 = \{1, \dots, k\}, \mathcal{K}_1 = \{k+1, \dots, 2k\}, \dots$; for M_2^{SS} , we use $\mathcal{K}_2 = \{2, \dots, k+1\}, \mathcal{K}_1 = \{k+2, \dots, 2d+1\}, \dots$; and so on. This leads to k bases M_i .

This procedure may leave a significant number of remaining terms, especially in the case of electronic structure. For example, any term that operates on qubits more than k indices apart will not be placed into any of the M_q partitions. Hence the remaining terms are partitioned using a different method; our implementation uses SortedInsertion with full commutation [7] on these remaining terms.

F. Index reordering

In electronic structure, the Jordan-Wigner transform yields long Pauli strings (*i.e.* terms with high Pauli weight). Because it will typically be easier to fill a partition M_q with many low-weight terms than with many high-weight terms, it will often be beneficial to re-order the electronic Hamiltonian (18). Intuitively, one would like to pack the more significant terms (those with larger $|t_{pq}|$ and $|t_{pqrs}|$) into as few partitions M_q as possible; hence one would like such terms with larger $|h|$ to have smaller Pauli weight. To this end we use the following cost function to optimize index ordering:

$$C_{\text{ordering}} = \sum_{pq} \|t_{pq}\| \|p - q\| + \sum_{pqrs} \|t_{pqrs}\| (\max(p, q, r, s) - \min(p, q, r, s)). \quad (22)$$

Optimizing with respect to this cost function ensures that, after the Jordan-Wigner transform, the more significant terms span fewer qubits. We implemented a simple reindexing algorithm as follows. First we swap a random pair of indices. The swap is kept only if C_{ordering} decreases; otherwise the indices are placed in their previous position. In our implementation, the algorithm is halted after some threshold of failed swaps in a row.

G. Partitioning via pre-encoded operators

Methods (such as our simple greedy algorithm above) that operate directly on the qubit space are unlikely to take advantage of much of the structure of the “pre-encoded” (*i.e.* expressed as bosonic or fermionic operators) Hamiltonian. In a sense this structure is lost or hidden after the problem is encoded to qubits. It may instead be useful to explicitly consider the pre-encoded operator, in order to directly take its particular tensor product structure into account. Let us assume that the pre-encoded Hamiltonian is known and is expressible as

$$H = \sum_i B_{i0}^{[k_{i0}]} \otimes B_{i1}^{[k_{i1}]} \otimes B_{i2}^{[k_{i2}]} \otimes \dots \quad (23)$$

where superscripts denote the logarithm of the size of each tensor. Then a greedy search algorithm may not be needed for k -NoCliD, as it may be more straightforward to use the components of (23) to intuitively construct the W_{gr} of equation (10). The benefits of this strategy are most obvious with Hamiltonians of bosonic (or phononic) degrees of freedom. The following three sections consider the structure of the pre-encoded operators when implementing a partitioning plan.

H. Lattice edge coloring

In lattice models, we propose using an edge coloring approach to arrive at a k -NoCliD factorization. Define \mathcal{E} to be the set of all edges in the lattice.

In the Bose-Hubbard model, in each edge coloring one can simultaneously measure all $b_i^\dagger b_j + b_i b_j^\dagger$ where edge (i, j) belongs to the same color. An edge coloring leads to sets of edges denoted $\mathcal{E}_1, \mathcal{E}_2, \dots, \mathcal{E}_{n_c}$ where n_c is the number of colors and $\bigcup_k \mathcal{E}_k = \mathcal{E}$. Then one measures in n_c bases

$$M_k^{\text{BH,hop}} = \sum_{\{(i,j)\} \in \mathcal{E}_k} \left(b_i^\dagger b_j + b_i b_j^\dagger \right) \quad (24)$$

where $\{i, j\}$ is an edge in the set \mathcal{E}_k . One also measures in the diagonal Z basis to recover all $n_i(n_i - 1)$ terms in equation (19), leading a total of just $n_c + 1$ bases in which to measure. $M_k^{\text{BH,hop}}$ requires diagonalization across two bosonic modes, *i.e.* the diagonalization parameter $k = 2 \log_2 d$. (In the next subsection we give a method that

allows k to be halved.) We summarize well-known results [59] for colorings of regular lattices in Table IIH.

Now we consider the one-dimensional spinless Fermi-Hubbard model with only nearest-neighbor interactions. Fermionic case 1D. Regardless of system size, only two 2-NoCliD bases are required:

$$\begin{aligned} M_0^{\text{FH,1D}} &= (tX_0X_1 + tY_0Y_1 - \frac{U}{8}Z_0Z_1 + \frac{U}{8}Z_0) \\ &\quad + (tX_2X_3 + tY_2Y_3 - \frac{U}{8}Z_2Z_3 + \frac{U}{8}Z_2) + \dots \\ M_1^{\text{FH,1D}} &= (tX_1X_2 + tY_1Y_2 - \frac{U}{8}Z_1Z_2 + \frac{U}{8}Z_1) \\ &\quad + (tX_3X_4 + tY_3Y_4 - \frac{U}{8}Z_3Z_4 + \frac{U}{8}Z_3) + \dots \end{aligned} \quad (25)$$

Hence one would diagonalize the 2-qubit operator $(tX_iX_j + tY_iY_j - \frac{U}{8}Z_iZ_j + \frac{U}{8}Z_i)$ simultaneously across $(i, j) \in ((0, 1), (2, 3), \dots)$, and then simultaneously across $(i, j) \in ((1, 2), (3, 4), \dots)$. Contrast this with commuting grouping methods, where one would need 3 bases: $XX + YY$ for two colors, and then Z for all sites. This smaller number of bases (two instead of three) is not guaranteed to produce lower shot counts, but it does provide one more option for basis measurement. A more complicated coloring scheme is also possible for higher-dimensional Fermi-Hubbard models. We summarize the number of colors (which is equivalent to the number of bases) for different lattice types in Table I, but we leave further details for future work.

	1D	Square	Hex	Triang.	Cubic	Tetrahed.
Colors	2	4	3	6	6	4

TABLE I. Number of colors in optimal edge coloring of different lattice types.

I. Products of one-body Hermitians

In the previous section we introduced a lattice coloring scheme, because hopping terms $b_i^\dagger b_j + b_i b_j^\dagger$ on adjacent edges cannot be simultaneously measured. Here we introduce a method to avoid coloring altogether, which results in a much lower (and in fact constant) number of measurement bases. The key insight is that the following equality holds:

$$b_i^\dagger b_j + h.c. = q_i q_j + p_i p_j. \quad (26)$$

The RHS is useful because (unlike the LHS) it is a *sum of products of one-body Hermitians*. (Such constructs are useful in other contexts in quantum algorithms for electronic structure [60].) Because the one-body non-Hermitian $\langle a_i^\dagger \rangle$ and $\langle a_i \rangle$ cannot be directly measured on a quantum computer, it would appear that the entire

two-body hopping term $\langle b_i^\dagger b_j + h.c. \rangle$ must be measured, which is why diagonalization must be across $k = 2 \log_2 d$ qubits.

But if we use the RHS of equation (26), we can simply measure q in *all* bases (with diagonalization across only $k = \log_2 d$ qubits), followed by p in all bases, leading to measurement basis operators

$$\begin{aligned} M_q^{\text{BH,quad}} &= \sum_{\{(i,j)\} \in \mathcal{E}} q_i q_j \\ M_p^{\text{BH,quad}} &= \sum_{\{(i,j)\} \in \mathcal{E}} p_i p_j \\ M_n^{\text{BH,quad}} &= \sum n_i. \end{aligned} \quad (27)$$

This is massively beneficial because we can now both (a) reduce k by half and (b) reduce the number of measurement bases to a constant of just three. This means we can measure in three bases *regardless of lattice type*, even an all-to-all lattice. Note that $M_n^{\text{BH,quad}}$ can be measured in the Z-basis without additional diagonalization circuit.

In the structure of vibrational Hamiltonians in the form of equation (20), the same strategy may be used. Analogously to the Bose-Hubbard case, one can measure a vibrational Hamiltonian using only *two* bases: q_1, q_2, \dots and p_1, p_2, \dots .

$$\begin{aligned} M_q^{\text{vibr}} &= \frac{1}{2} \sum_i^M \omega_i q_i^2 + \sum_{\{ijk\}} c_{ijk} q_i q_j q_k \\ &\quad + \sum_{\{ijkl\}} c_{ijkl} q_i q_j q_k q_l + \dots \\ M_p^{\text{vibr}} &= \frac{1}{2} \sum_i^M \omega_i p_i^2 \end{aligned} \quad (28)$$

Each $A_{qrs}^{\mathcal{K}}$ in equation (10) is simply a q or p , and all q -containing tensor products in equation (20) can be measured simultaneously, regardless of order or of number of terms. Hence any vibrational Hamiltonian of form (20) may be measured in just *two* bases.

J. Sub-operators

In previous sections we have implicitly required diagonalization circuits over k qubits, where k is often determined by the problem of interest (mainly via the truncation of the bosonic or phononic modes). This is allowable because k is small for many if not most applications: low-temperature Bose-Hubbard simulations usually can use truncations less than $d = 8$ ($k=3$), and many molecules of interest do not require vibrational cutoffs of more than $d = 16$ ($k=4$). Hence we do not often expect circuit depths to be an obstacle. However, there will be cases where a large k requires circuit depths that are too high.

In such cases, one needs to split the original k' -local operators into tensor decompositions with tensor size $k <$

k' . We decompose the tensors in equation (10) as

$$A_{qrs} \rightarrow \sum_l \bigotimes_m \hat{a}_{qrslm} \quad (29)$$

such that all \hat{a} operate on $\leq k'$ qubits. This construction is more relevant to bosonic and phononic Hamiltonians, because in the fermionic case one tunes k using unrelated methods as discussed below.

This sub-operator decomposition allows one to use the methods of the previous two sections, while still imposing arbitrarily small k . Now that one is measuring each term in the new decomposition separately, an edge coloring is again required even for the one-body Hermitian string strategy, which was not that case if $k' = k$. We leave a more thorough treatment of this sub-operator strategy to future work.

III. NUMERICAL RESULTS

Here we present numerical results for shot counts, for four Hamiltonian classes. Note that in the interest of rigor, we calculate exact shot counts N , circumventing useful but order-of-magnitude approximations like the \hat{R} metric [7]. Hence our simulations do not exceed 16 qubits. We run the algorithms on random quantum states and report results in terms of $\varepsilon^2 N$ (see (3)), which we refer to as the measurement variance. Where index reordering was performed, the algorithm was halted after 5000 failed swaps in a row. Hamiltonians were taken from the HamLib dataset [61, 62] or produced using software packages OpenFermion [63] and mat2qubit [64].

QWC-SI and FC-SI denote qubit-wise commutation and full commutation, both using SortedInsertion as the partitioning algorithm. Lower bounds are calculated by diagonalizing the full Hamiltonian; in other words, implementing formula (3) with a single fragment. Greedy, Blocked, and Coloring denote the methods of Sections IID, IIE, and IIH, respectively. QPN and QP denote the method of Section III, using measurement bases $\{q_i, p_i, n_i\}$ and $\{q_i, p_i\}$, respectively.

For the spinless Fermi-Hubbard model (Figure 1), the NoCliD-coloring method out-performs SortedInsertion, though they are comparable in magnitude. However, that these results are for $k = 2$ as in equation (25), shows that the improvement in shot counts is achieved at negligible cost in circuit depth.

For electronic structure, because of the higher Pauli weights, we do not expect these rudimentary partition algorithms to easily out-perform FC-SI. However, we were interested in demonstrating *some* threshold value of k^* beyond which NoCliD leads to a shot count lower than FC-SI. We found $k^*=6$ for LiH, $k^*=7$ for HF, NH, and NaLi, $k^*=8$ for BH, C2, F2, H6, O2, and OH, $k^*=9$ for B2, BeH, CH, and Na2, and $k^*=10$ for N2, where Hamiltonians were taken from HamLib. In these cases, unlike in the bosonic cases, NoCliD-blocking performed slightly worse than NoCliD-greedy. We stress that the “disjoint”

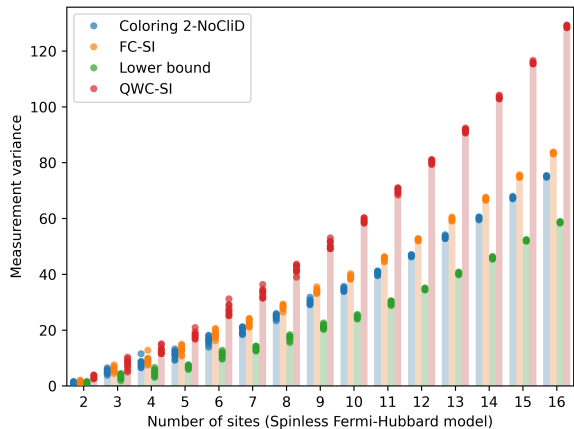


FIG. 1. Measurement variance $\varepsilon^2 N$ for the spinless Fermi-Hubbard model.

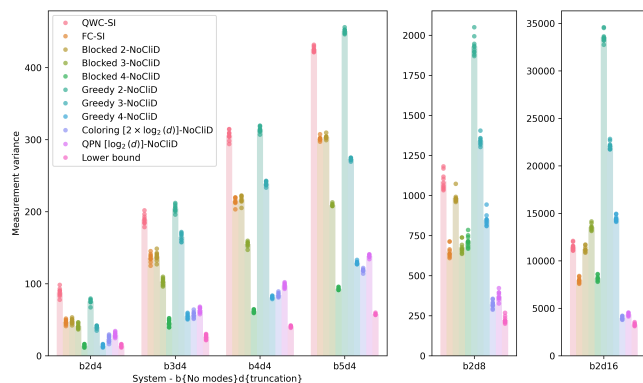


FIG. 2. Measurement variance $\varepsilon^2 N$ for the Bose-Hubbard model. Labels denote the number of bosonic modes and the bosonic truncation. For example, b3d4 signifies 3 bosonic modes with a truncation of $d = 4$ in each mode.

constraint of Section IID’s greedy algorithm is extremely restrictive, likely leading to far more partitions than necessary. This threshold for k is likely to be significantly reduced in electronic structure Hamiltonians by relaxing this constraint, and we leave this as a direction for future work.

Across all considered instances of Bose-Hubbard (Figure 2), k -NoCliD methods consistently outperform traditional methods. When comparing coloring and QPN methods, QPN is slightly superior in most cases. Given that QPN achieves this performance with k values half as large, it is recommended as the preferred method. Additionally, methods like greedy and blocking, which do not account for the original Hamiltonian structure, are inferior to both coloring and QPN approaches. This is unsurprising, as the latter methods explicitly consider the bosonic structure of the problem.

Finally, for vibrational structure (Figure 3), all NoCliD methods outperform the traditional SortedInsertion ap-

proach. Similar to the Bose-Hubbard case, the blocking and greedy methods are easily outperformed by the QP method, as they fail to account for the bosonic structure. The QP method also performs very close to the theoretical lower bound, which is perhaps unsurprising as it requires only two bases regardless of the Hamiltonian instance. These results are nearly optimal as they are very close to the lower bound of diagonalizing the full Hamiltonian, vastly out-performing all methods. This is an especially notable results considering that k is very small ($k = 2$) for these QP results.

In all four Hamiltonian classes, at least one k -NoCliD partitioning strategy led to smaller measurement variance with respect to SortedInsertion with qubit-wise commutation (QWC) and full commutation (FC). The largest improvements were observed for bosonic and phononic degrees of freedom even for very small k , partly because these Hamiltonians tend to have shorter Pauli products in qubit space and partly because it is easier to tailor k -NoCliD to these Hamiltonians than to electronic structure. For large enough k , k -NoCliD leads to fewer shots even for electronic structure, though future work is needed to reduce this threshold value of k .

IV. CONCLUSIONS

We introduced a class of methods for reducing shot counts in expectation value estimation. Our approach, referred to as k -local non-Clifford diagonalization (k -NoCliD), allows for partitioning of arbitrary terms, as long as the size of each tensor in the tensor product operates on at most k qubits. As the basis-change circuit depth increases with k , the method allows for a natural trade-off between shot counts and circuit depth. We calculated exact shot counts required for four Hamiltonian classes: Bose-Hubbard, Fermi-Hubbard, vibrational structure, and electronic structure. In all cases, there is some value of k for which k -NoCliD out-performs other partitioning methods based on mutually commuting partitions.

For now, the method’s utility is clearest for vibrational, bosonic, and Fermi-Hubbard Hamiltonians, where the method often out-performs fully-commuting methods by k as small as 2 (for which the basis change circuit is extremely shallow). These positive results are largely due to the fact that we developed specialized partitioning algorithms for these Hamiltonians. For electronic structure, we left the development of more sophisticated partitioning methods to future work, which we expect to drastically reduce the threshold value of k . Other future research directions include extensions of the method based on ‘ghost’ [18] and ‘fluid’ [19] partitioning methods introduced previously, as well as a thorough study of the basis-change quantum circuits.

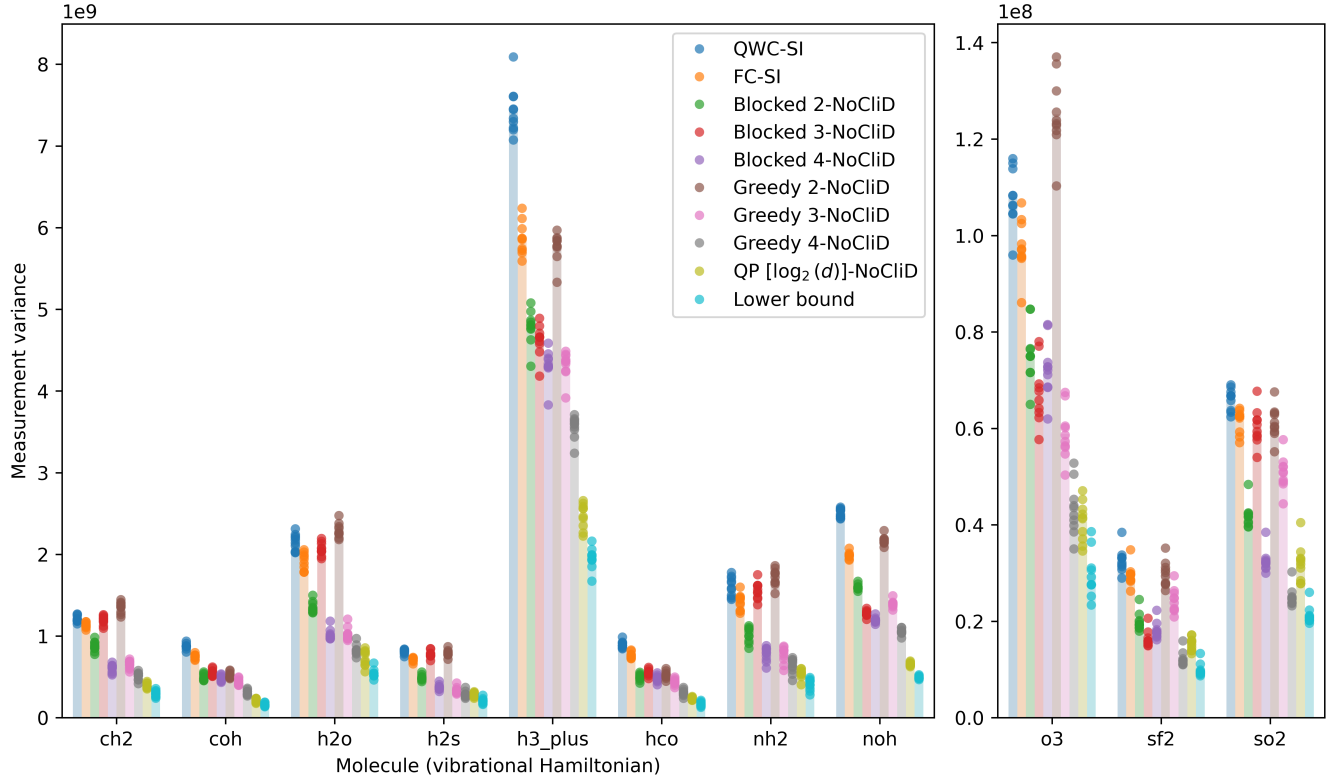


FIG. 3. Measurement variance $\varepsilon^2 N$ for molecular vibrational structure in units cm^{-2} , where all modes in the model are truncated as $d = 4$.

ACKNOWLEDGEMENTS

This research used resources of the National Energy Research Scientific Computing Center (NERSC), a Department of Energy Office of Science User Facility using NERSC awards ASCR-ERCAP0029116, DDR-ERCAP0030342, and DDR-ERCAP0033798. This work was supported by Wellcome Leap as part of the Quantum for Bio Program.

Appendix A: Valid and invalid tensor products for k -NoCliD

In order to build some intuition for allowable fragments in k -NoCliD, here we show some examples of valid Pauli string matchings for a given k . “Matched” local operators are denoted with blue.

For $k=1$, an example of a valid string matching set is $\{aXXZ, bXXY\}$. Another example is $\{aIZI, bXI\}$. That diagonalizing qubit is denoted in blue. Note that unlike in commuting set methods, in the general case real coefficients a, b, \dots need to be included in the definition; though this is not strictly required for the basic versions of k -NoCliD, it will be required for the more complicated factoring methods discussed below.

For $k=2$, examples of valid string matchings are $\{$

$aIXXI, bIXXI\}$ and $\{aIZIZI, bIXI\}$. Note that the local operator on black qubits must match exactly, while there is complete freedom for the blue qubits.

The point is, the overall operator must be able to be factored into a tensor product of operators as in equation (10), where each operator in the tensor product operates on at most k qubits.

Non-examples. Here are some examples of *invalid* string-matching. Some non-examples of partitionings for $k=1$ are $\{aIXXZ, bXXXI\}$ and even $\{aIXXZ, bXXXI\}$, where non-identical local operators are in gray (these are valid $k=2$ matchings but invalid $k=1$ matchings). It is important to consider the latter set; it shows that even if a set is k -qubitwise-commuting, that does not make it a valid k -NoCliD matching. This highlights the fact that, unlike in the case of commuting grouping, k -NoCliD indeed requires that the operator be representable as equation (10) such that all $k_i < k$.

For $k=1$, another example of an *invalid* string matching is XIX and IXZ . Even though the first two qubit qubitwise commute, the set cannot be expressed as a product of tensors each operating on at most 1 qubit.

Appendix B: Proof of 1-qubit basis change result

Before proceeding to the proof of Result 1, we begin this section with two examples in order to build intuition.

Consider the following pedagogical Hamiltonian,

$$H_1 = \frac{1}{\sqrt{2}}X + \frac{1}{\sqrt{2}}Z. \quad (\text{B1})$$

We refer to the basis in which equation (B1) is defined as the global Pauli basis (GPB).

We define $P_O \equiv \mathcal{N}O$ for any one-qubit Hermitian operator O , where \mathcal{N} is a normalization constant such that $P_O^2 = I$. In other words, P_O is a rotated Pauli matrix. For Hamiltonian H_1 , we use

$$P_{X+Z} = (X + Z)/\sqrt{2} \quad (\text{B2})$$

The point is to measure in the P_{X+Z} basis directly instead of measuring in the X or Z Pauli bases. For one qubit, this entails simply rotating on the Bloch sphere to an orientation halfway between the X and Z axes. We note that, by definition, the following properties are true for all P_O :

$$\begin{aligned} \text{Var}[P] &= \langle P^2 \rangle - \langle P \rangle^2 \\ \text{Var}[P] &= 1 - \langle P \rangle^2 \end{aligned} \quad (\text{B3})$$

Now we consider the total number of measurements required to calculate $\langle H_1 \rangle$ for two distinct states: $|\phi\rangle = R_y(\pi/4)|0\rangle \approx [0.924, 0.383]^T$ and $|0\rangle$. For each state we consider measuring in (a) the global Pauli basis (GPB) (which is restricted for measuring only $\langle X \rangle$ and $\langle Z \rangle$) and (b) the $\langle P_{X+Z} | P_{X+Z} \rangle$ basis which we refer to as the rotated basis (RB).

Note that

$$R_y(\theta) = \begin{bmatrix} \cos(\theta/2) & -\sin(\theta/2) \\ \sin(\theta/2) & \cos(\theta/2) \end{bmatrix} \quad (\text{B4})$$

Measuring $\langle \phi | A | \phi \rangle$ in the global Pauli basis yields:

$$\begin{aligned} \varepsilon^2 N_{tot}^{GPB} &= \left(\sqrt{\text{Var}[\frac{1}{\sqrt{2}}X]} + \sqrt{\text{Var}[\frac{1}{\sqrt{2}}Z]} \right)^2 \\ &= \left(\sqrt{\frac{1}{2}(1 - \langle \phi | X | \phi \rangle^2)} + \sqrt{\frac{1}{2}(1 - \langle \phi | Z | \phi \rangle^2)} \right)^2 \\ &= \left(\sqrt{\frac{1}{2}(1 - \frac{1}{2})} + \sqrt{\frac{1}{2}(1 - \frac{1}{2})} \right)^2 \\ &= 1 \end{aligned} \quad (\text{B5})$$

Measuring $\langle \phi | A | \phi \rangle$ in the RB basis P_{X+Z} yields:

$$\begin{aligned} \varepsilon^2 N_{tot}^{RB} &= \text{Var}[\langle \phi | P_{X+Z} | \phi \rangle] \\ &= (1 - \langle \phi | P_{X+Z} | \phi \rangle^2) \\ &= (1 - 1) \\ &= 0 < \varepsilon^2 N_{tot}^{GPB} \end{aligned} \quad (\text{B6})$$

So for this example state $|\phi\rangle$ it is indeed beneficial to move to the rotated basis. This is expected, as $|\phi\rangle$ is an eigenfunction of H_1 .

Now we instead consider $\langle 0 | A | 0 \rangle$. $\langle 0 | A | 0 \rangle$ in the Pauli basis yields:

$$\begin{aligned} \varepsilon^2 N_{tot}^{GPB} &= \left(\sqrt{\text{Var}[\frac{1}{\sqrt{2}}X]} + \sqrt{\text{Var}[\frac{1}{\sqrt{2}}Z]} \right)^2 \\ &= \left(\sqrt{\frac{1}{2}(1 - \langle 0 | X | 0 \rangle^2)} + \sqrt{\frac{1}{2}(1 - \langle 0 | Z | 0 \rangle^2)} \right)^2 \\ &= \left(\sqrt{\frac{1}{2}(1 - 1)} + \sqrt{\frac{1}{2}(1 - 0)} \right)^2 \\ &= (0 - \frac{1}{\sqrt{2}})^2 \\ &= \frac{1}{2} \end{aligned} \quad (\text{B7})$$

Measuring $\langle 0 | A | 0 \rangle$ in the RB basis P_{X+Z} yields:

$$\begin{aligned} \varepsilon^2 N_{tot}^{RB} &= \text{Var}[\langle 0 | P_{X+Z} | 0 \rangle] \\ &= (1 - \langle 0 | P_{X+Z} | 0 \rangle^2) \\ &= (1 - (\frac{1}{\sqrt{2}})^2) \\ &= \frac{1}{2} \end{aligned} \quad (\text{B8})$$

where we have used

$$P_{X+Z} = \frac{1}{\sqrt{2}} \begin{bmatrix} 1 & 1 \\ 1 & -1 \end{bmatrix} \quad (\text{B9})$$

So in the particular case of $\langle 0 | H_1 | 0 \rangle$, we see that $N_{tot}^{GPB} = N_{tot}^{RB}$. Both bases yield the same measurement counts in this case.

We have seen in the two examples above that M_{RB} is either less than or equal to M_{GPB} . We now prove that this is the case for any one-qubit real operator and real state. The purpose of this is to show that moving to the rotated basis (RB) is always beneficial or neutral, in terms of shot counts, for this general case.

What follows is a proof of Result 1.

Proof. Expressing a general real state as

$$|\psi_\alpha\rangle = \alpha|0\rangle + \sqrt{1 - \alpha^2}|1\rangle$$

it follows that

$$\begin{aligned} \langle \psi_\alpha | H(\eta) | \psi_\alpha \rangle &= \alpha(\alpha\sqrt{1 - \eta^2}\eta\sqrt{1 - \alpha^2}) \\ &\quad + \sqrt{1 - \alpha^2}(\alpha\eta - \sqrt{1 - \alpha^2}\sqrt{1 - \eta^2}). \end{aligned} \quad (\text{B10})$$

We have

$$\varepsilon^2 M^{RB} = \langle \psi_\alpha | P_H(\eta) | \psi_\alpha \rangle = \langle \psi_\alpha | H(\eta) | \psi_\alpha \rangle$$

where the second equality is true simply because the one-qubit Hamiltonian H has unit norm. Next we write down

$$\begin{aligned}\varepsilon^2 M^{GPB} &= \left(\sqrt{\text{Var}[\eta X]} + \sqrt{\text{Var}[\sqrt{1-\eta^2} Z]} \right)^2 \\ &= \left(\eta \sqrt{\text{Var}[X]} + \sqrt{1-\eta^2} \sqrt{\text{Var}[Z]} \right)^2\end{aligned}\quad (\text{B11})$$

Straightforward algebra yields

$$\begin{aligned}\varepsilon^2 M^{GPB} - \varepsilon^2 M^{RB} &= (8\alpha^3\eta - 4\alpha\eta) \sqrt{1-\alpha^2} \sqrt{1-\eta^2} \\ &\quad + 8\eta \sqrt{1-\eta^2} \sqrt{-\alpha^4 + \alpha^2} \sqrt{\alpha^4 - \alpha^2 + \frac{1}{4}},\end{aligned}\quad (\text{B12})$$

which is ≥ 0 for all $\eta, \alpha \in [0, 1]$. \square

-
- [1] Sam McArdle, Suguru Endo, Alán Aspuru-Guzik, Simon C. Benjamin, and Xiao Yuan. Quantum computational chemistry. *Rev. Mod. Phys.*, 92:015003, Mar 2020.
- [2] Bela Bauer, Sergey Bravyi, Mario Motta, and Garnet Kin-Lic Chan. Quantum algorithms for quantum chemistry and quantum materials science. *Chemical Reviews*, 120(22):12685–12717, Nov 2020.
- [3] Katherine Klymko, Carlos Mejuto-Zaera, Stephen J. Cotton, Filip Wudarski, Miroslav Urbanek, Diptarka Hait, Martin Head-Gordon, K. Birgitta Whaley, Jonathan Moussa, Nathan Wiebe, Wibe A. de Jong, and Norm M. Tubman. Real-time evolution for ultracompact hamiltonian eigenstates on quantum hardware. *PRX Quantum*, 3:020323, May 2022.
- [4] Yuri Alexeev, Maximilian Amsler, Marco Antonio Barroca, Sanzio Bassini, Torey Battelle, Daan Camps, David Casanova, Young Jay Choi, Frederic T Chong, Charles Chung, et al. Quantum-centric supercomputing for materials science: A perspective on challenges and future directions. *Future Generation Computer Systems*, 160:666–710, 2024.
- [5] Abid Khan, Prateek Vaish, Yaoqi Pang, Nikhil Kowshik, Michael S. Chen, Clay H. Batton, Grant M. Rotskoff, J. Wayne Mullinax, Bryan K. Clark, Brenda M. Rubenstein, and Norm M. Tubman. Quantum Hardware-Enabled Molecular Dynamics via Transfer Learning. arXiv e-prints, page arXiv:2406.08554, June 2024.
- [6] Janus J Eriksen, Tyler A Anderson, J Emiliano Deustua, Khaldoon Ghanem, Diptarka Hait, Mark R Hoffmann, Seunghoon Lee, Daniel S Levine, Ilias Magoulas, Jun Shen, et al. The ground state electronic energy of benzene. *The journal of physical chemistry letters*, 11(20):8922–8929, 2020.
- [7] Ophelia Crawford, Barnaby van Straaten, Daochen Wang, Thomas Parks, Earl Campbell, and Stephen Brierley. Efficient quantum measurement of pauli operators in the presence of finite sampling error. *Quantum*, 5:385, 2021.
- [8] Jérôme F Gonthier, Maxwell D Radin, Corneliu Buda, Eric J Daskocil, Clena M Abuan, and Jhonathan Romero. Measurements as a roadblock to near-term practical quantum advantage in chemistry: Resource analysis. *Physical Review Research*, 4(3):033154, 2022.
- [9] Tzu-Ching Yen, Aadithya Ganeshram, and Artur F. Izmaylov. Deterministic improvements of quantum measurements with grouping of compatible operators, non-local transformations, and covariance estimates. *npj Quantum Information*, 9(1):14, February 2023.
- [10] Erik J. Gustafson, Juha Tiihonen, Diana Chamaki, Farshud Sorourifar, J. Wayne Mullinax, Andy C. Y. Li, Filip B. Maciejewski, Nicolas PD Sawaya, Jaron T. Krogel, David E. Bernal Neira, and Norm M. Tubman. Surrogate optimization of variational quantum circuits, 2024.
- [11] Artur F Izmaylov, Tzu-Ching Yen, Robert A Lang, and Vladyslav Verteletskyi. Unitary partitioning approach to the measurement problem in the variational quantum eigensolver method. *Journal of chemical theory and computation*, 16(1):190–195, 2019.
- [12] Vladyslav Verteletskyi, Tzu-Ching Yen, and Artur F. Izmaylov. Measurement optimization in the variational quantum eigensolver using a minimum clique cover. *The Journal of Chemical Physics*, 152(12):124114, March 2020.
- [13] Pranav Gokhale, Olivia Angiuli, Yongshan Ding, Kaiwen Gui, Teague Tomesh, Martin Suchara, Margaret Martonosi, and Frederic T Chong. $O(n^3)$ measurement cost for variational quantum eigensolver on molecular hamiltonians. *IEEE Transactions on Quantum Engineering*, 1:1–24, 2020.
- [14] Andrew Zhao, Andrew Tranter, William M Kirby, Shu Fay Ung, Akimasa Miyake, and Peter J Love. Measurement reduction in variational quantum algorithms. *Physical Review A*, 101(6):062322, 2020.
- [15] Hsin-Yuan Huang, Richard Kueng, and John Preskill. Predicting many properties of a quantum system from very few measurements. *Nature Physics*, 16(10):1050–1057, 2020.
- [16] Tzu-Ching Yen and Artur F. Izmaylov. Cartan Subalgebra Approach to Efficient Measurements of Quantum Observables. *PRX Quantum*, 2(4):040320, October 2021.
- [17] William J Huggins, Jarrod R McClean, Nicholas C Rubin, Zhang Jiang, Nathan Wiebe, K Birgitta Whaley, and Ryan Babbush. Efficient and noise resilient measurements for quantum chemistry on near-term quantum computers. *npj Quantum Information*, 7(1):23, 2021.
- [18] Seonghoon Choi, Tzu-Ching Yen, and Artur F. Izmaylov. Improving quantum measurements by introducing "ghost" Pauli products. *Journal of Chemical Theory and Computation*, 18(12):7394–7402, December 2022. arXiv:2208.06563 [physics, physics:quant-ph].
- [19] Seonghoon Choi, Ignacio Loaiza, and Artur F. Izmaylov. Fluid fermionic fragments for optimizing quantum measurements of electronic Hamiltonians in the variational quantum eigensolver. *Quantum*, 7:889, January 2023. arXiv:2208.14490 [physics, physics:quant-ph].

- [20] Marco Majland, Rasmus Berg Jensen, Mads Greisen Højlund, Nikolaj Thomas Zinner, and Ove Christiansen. Optimizing the number of measurements for vibrational structure on quantum computers: coordinates and measurement schemes. *Chemical Science*, 14(28):7733–7742, 2023.
- [21] Arkopal Dutt, William Kirby, Rudy Raymond, Charles Hadfield, Sarah Sheldon, Isaac L Chuang, and Antonio Mezzacapo. Practical benchmarking of randomized measurement methods for quantum chemistry hamiltonians. *arXiv preprint arXiv:2312.07497*, 2023.
- [22] Ben DalFavero, Rahul Sarkar, Daan Camps, Nicolas Sawaya, and Ryan LaRose. k -commutativity and measurement reduction for expectation values. *arXiv preprint arXiv:2312.11840*, 2023.
- [23] Xavier Bonet-Monroig, Ryan Babbush, and Thomas E O’Brien. Nearly optimal measurement scheduling for partial tomography of quantum states. *Physical Review X*, 10(3):031064, 2020.
- [24] Wataru Inoue, Koki Aoyama, Yusuke Teranishi, Keita Kanno, Yuya O Nakagawa, and Kosuke Mitarai. Almost optimal measurement scheduling of molecular hamiltonian via finite projective plane. *Physical Review Research*, 6(1):013096, 2024.
- [25] Emanuel Knill, Gerardo Ortiz, and Rolando D Somma. Optimal quantum measurements of expectation values of observables. *Physical Review A—Atomic, Molecular, and Optical Physics*, 75(1):012328, 2007.
- [26] Thomas E O’Brien, Michael Streif, Nicholas C Rubin, Raffaele Santagati, Yuan Su, William J Huggins, Joshua J Goings, Nikolaj Moll, Elica Kyoseva, Matthias Degroote, et al. Efficient quantum computation of molecular forces and other energy gradients. *Physical Review Research*, 4(4):043210, 2022.
- [27] Mark Steudtner, Sam Morley-Short, William Pol, Sukin Sim, Cristian L Cortes, Matthias Loipersberger, Robert M Parrish, Matthias Degroote, Nikolaj Moll, Raffaele Santagati, et al. Fault-tolerant quantum computation of molecular observables. *Quantum*, 7:1164, 2023.
- [28] Jarrod R McClean, Jonathan Romero, Ryan Babbush, and Alán Aspuru-Guzik. The theory of variational hybrid quantum-classical algorithms. *New Journal of Physics*, 18(2):023023, 2016.
- [29] Scott Aaronson and Daniel Gottesman. Improved simulation of stabilizer circuits. *Physical Review A*, 70(5):052328, November 2004.
- [30] Emanuel Knill. Approximation by quantum circuits. *arXiv preprint quant-ph/9508006*, 1995.
- [31] Raban Iten, Roger Colbeck, Ivan Kukuljan, Jonathan Home, and Matthias Christandl. Quantum circuits for isometries. *Physical Review A*, 93(3):032318, 2016.
- [32] Ed Younis, Costin C Iancu, Wim Lavrijsen, Marc Davis, Ethan Smith, and USDOE. Berkeley quantum synthesis toolkit (bqskit) v1, 4 2021.
- [33] Daniel S Abrams and Seth Lloyd. Simulation of many-body fermi systems on a universal quantum computer. *Physical Review Letters*, 79(13):2586, 1997.
- [34] Chris Cade, Lana Mineh, Ashley Montanaro, and Stasja Stanisic. Strategies for solving the fermi-hubbard model on near-term quantum computers. *Physical Review B*, 102(23):235122, 2020.
- [35] James PF LeBlanc, Andrey E Antipov, Federico Becca, Ireneusz W Bulik, Garnet Kin-Lic Chan, Chia-Min Chung, Youjin Deng, Michel Ferrero, Thomas M Henderson, Carlos A Jiménez-Hoyos, et al. Solutions of the two-dimensional hubbard model: benchmarks and results from a wide range of numerical algorithms. *Physical Review X*, 5(4):041041, 2015.
- [36] James D Whitfield, Jacob Biamonte, and Alán Aspuru-Guzik. Simulation of electronic structure hamiltonians using quantum computers. *Molecular Physics*, 109(5):735–750, 2011.
- [37] Ryan Babbush, Jarrod McClean, Dave Wecker, Alán Aspuru-Guzik, and Nathan Wiebe. Chemical basis of trotter-suzuki errors in quantum chemistry simulation. *Physical Review A*, 91(2):022311, 2015.
- [38] N Elstner and H Monien. Dynamics and thermodynamics of the bose-hubbard model. *Physical Review B*, 59(19):12184, 1999.
- [39] Rolando Somma, Gerardo Ortiz, Emanuel Knill, and James Gubernatis. Quantum simulations of physics problems. *International Journal of Quantum Information*, 1(02):189–206, 2003.
- [40] Sina Bahrami and Nicolas Sawaya. Particle-conserving quantum circuit ansatz with applications in variational simulation of bosonic systems. *arXiv preprint arXiv:2402.18768*, 2024.
- [41] Sam McArdle, Alexander Mayorov, Xiao Shan, Simon Benjamin, and Xiao Yuan. Digital quantum simulation of molecular vibrations. *Chemical science*, 10(22):5725–5735, 2019.
- [42] Pauline J Ollitrault, Alberto Baiardi, Markus Reiher, and Ivano Tavernelli. Hardware efficient quantum algorithms for vibrational structure calculations. *Chemical science*, 11(26):6842–6855, 2020.
- [43] Hamza Jnane, Nicolas PD Sawaya, Borja Peropadre, Alan Aspuru-Guzik, Raul Garcia-Patron, and Joonsuk Huh. Analog quantum simulation of non-condon effects in molecular spectroscopy. *ACS Photonics*, 8(7):2007–2016, 2021.
- [44] Nicolas PD Sawaya and Joonsuk Huh. Improved resource-tunable near-term quantum algorithms for transition probabilities, with applications in physics and variational quantum linear algebra. *Advanced Quantum Technologies*, 6(9):2300042, 2023.
- [45] Nicolas PD Sawaya, Francesco Paesani, and Daniel P Tabor. Near-and long-term quantum algorithmic approaches for vibrational spectroscopy. *Physical Review A*, 104(6):062419, 2021.
- [46] Rolando D Somma. Quantum computation, complexity, and many-body physics. *arXiv preprint quant-ph/0512209*, 2005.
- [47] Sam McArdle, Alexander Mayorov, Xiao Shan, Simon Benjamin, and Xiao Yuan. Digital quantum simulation of molecular vibrations. *Chemical science*, 10(22):5725–5735, 2019.
- [48] Nicolas PD Sawaya, Albert T Schmitz, and Stuart Hadfield. Encoding trade-offs and design toolkits in quantum algorithms for discrete optimization: coloring, routing, scheduling, and other problems. *arXiv preprint arXiv:2203.14432*, 2022.
- [49] Nicolas PD Sawaya, Tim Menke, Thi Ha Kyaw, Sonika Johri, Alán Aspuru-Guzik, and Gian Giacomo Guerreschi. Resource-efficient digital quantum simulation of d-level systems for photonic, vibrational, and spins hamiltonians. *npj Quantum Information*, 6(1):1–13, 2020.
- [50] Nicolas PD Sawaya, Gian Giacomo Guerreschi, and

- Adam Holmes. On connectivity-dependent resource requirements for digital quantum simulation of d-level particles. In 2020 IEEE International Conference on Quantum Computing and Engineering (QCE), pages 180–190. IEEE, 2020.
- [51] Nan Jiang, Jian Wang, and Yue Mu. Quantum image scaling up based on nearest-neighbor interpolation with integer scaling ratio. Quantum information processing, 14(11):4001–4026, 2015.
- [52] Michael Lubasch, Jaewoo Joo, Pierre Moinier, Martin Kiffner, and Dieter Jaksch. Variational quantum algorithms for nonlinear problems. Physical Review A, 101(1):010301, 2020.
- [53] Ryan LaRose and Brian Coyle. Robust data encodings for quantum classifiers. Physical Review A, 102(3):032420, 2020.
- [54] Maria Schuld, Ryan Sweke, and Johannes Jakob Meyer. Effect of data encoding on the expressive power of variational quantum-machine-learning models. Physical Review A, 103(3):032430, 2021.
- [55] Xiaosi Xu, Jinzhao Sun, Suguru Endo, Ying Li, Simon C Benjamin, and Xiao Yuan. Variational algorithms for linear algebra. Science Bulletin, 66(21):2181–2188, 2021.
- [56] Mercy G Amankwah, Daan Camps, E Wes Bethel, Roel Van Beeumen, and Talita Perciano. Quantum pixel representations and compression for n-dimensional images. Scientific reports, 12(1):7712, 2022.
- [57] Raghav Jumade and Nicolas PD Sawaya. Data is often loadable in short depth: Quantum circuits from tensor networks for finance, images, fluids, and proteins. arXiv preprint arXiv:2309.13108, 2023.
- [58] Carlos Bravo-Prieto, Ryan LaRose, Marco Cerezo, Yigit Subasi, Lukasz Cincio, and Patrick J Coles. Variational quantum linear solver. Quantum, 7:1188, 2023.
- [59] Joris Kattemölle. Edge coloring lattice graphs. arXiv preprint arXiv:2402.08752, 2024.
- [60] Mario Motta, Kevin J Sung, K Birgitta Whaley, Martin Head-Gordon, and James Shee. Bridging physical intuition and hardware efficiency for correlated electronic states: the local unitary cluster jastrow ansatz for electronic structure. Chemical Science, 14(40):11213–11227, 2023.
- [61] Nicolas PD Sawaya, Daniel Marti-Dafcik, Yang Ho, Daniel P. Tabor, David Bernal, Alicia B. Magann, Shavindra Premaratne, Pradeep Dubey, Anne Matsuura, Nathan Bishop, Wibe A. de Jong, Simon Benjamin, Ojas D. Parekh, Norm Tubman, Katherine Klymko, and Daan Camps. Hamlib: A library of hamiltonians for benchmarking quantum algorithms and hardware, June 2023.
- [62] Anastasiia Butko, Katherine Klymko, Daan Camps, and Nicolas Sawaya. Hamperf: A hamiltonian-oriented approach to quantum benchmarking. In Proceedings of the 21st ACM International Conference on Computing Frontiers: Workshops and Special Sessions, pages 133–138, 2024.
- [63] Jarrod R McClean, Nicholas C Rubin, Kevin J Sung, Ian D Kivlichan, Xavier Bonet-Monroig, Yudong Cao, Chengyu Dai, E Schuyler Fried, Craig Gidney, Brendan Gimby, et al. Openfermion: the electronic structure package for quantum computers. Quantum Science and Technology, 5(3):034014, 2020.
- [64] Nicolas PD Sawaya. mat2qubit: A lightweight pythonic package for qubit encodings of vibrational, bosonic, graph coloring, routing, scheduling, and general matrix problems. arXiv preprint arXiv:2205.09776, 2022.